Four-phonon scattering in superfluid ^{4}He

1992 J. Phys.: Condens. Matter 4 7745

(http://iopscience.iop.org/0953-8984/4/38/008)

J. Phys.: Condens. Matter 4 (1992) 7745–7758. Printed in the UK

Four-phonon scattering in superfluid ^{4}He

M A H Tucker and A F G Wyatt
Department of Physics, University of Exeter, Stocker Road, Exeter EX4 4QL, UK

Received 11 June 1992

Abstract. The scattering of high-frequency ($\hbar\omega/k_B > 10$ K) phonons injected into superfluid ^{4}He with low-frequency ($\hbar\omega/k_B < 1$ K) thermal phonons in the liquid is studied both experimentally and theoretically. Quantum evaporation enables the selective study of only the high-frequency phonons. The attenuation of evaporation signals as the temperature is increased from 70 mK to 250 mK for various liquid path lengths is interpreted in terms of four-phonon scattering involving the high-frequency injected phonons and the low-frequency thermal phonons. Monte Carlo simulations of the signal variation with temperature show that the measured scattering is much weaker than the hydrodynamic theory has previously predicted. However, when this theory is extended to include diagrams representing further possible routes of the four-phonon scattering process, there are significant cancellations between these extra diagrams and those considered earlier. This leads to a weaker interaction and to a much improved agreement with the experimental results.

1. Introduction

The scattering between phonons in solids enables the phonons to come into equilibrium and also accounts for the thermal resistance of pure insulating crystals. The dominant scattering process involves three phonons (3PP) with energy conservation $\omega_1 \leftrightarrow \omega_2 + \omega_3$ and crystal momentum conservation $k_1 \leftrightarrow k_2 + k_3 + G$ where G is a reciprocal-lattice vector. Scattering involving four phonons (4PP) contributes only a small fraction to the phonon lifetime and so the 4PP has not yet been measured and related to theory [1]. Comparisons between theory and experiment are also complicated by the presence of impurities and crystal defects in real solids. A study of four-phonon scattering requires a medium that is very pure, free from defects, and where the three-phonon process is inhibited.

Superfluid ^{4}He (He II) is an almost ideal medium in which phonon propagation may be studied, uncomplicated by the structural defects and anisotropy inherent in solids, and has a range of phonon frequencies where the 3PP is not allowed. Only longitudinal phonons are present because the liquid cannot support transverse polarizations. At low temperatures, a phonon distribution injected into He II splits into a high-frequency ($\hbar\omega/k_B > 10$ K) and a low-frequency distribution because phonons with ($\hbar\omega/k_B < 10$ K) are unstable against decay [2]. This is due to the anomalous behaviour (upward curvature) of the dispersion curve at low frequencies. For low-frequency phonons, the situation is similar to that in solids, with the 3PP completely masking the 4PP at zero pressure. However, for the high-frequency phonons ($\hbar\omega/k_B > 10$ K), the 3PP is not allowed and the 4PP becomes the dominant process.

0953-8984/92/387745+14$04.50

As we can readily study these high-frequency phonons by 'quantum evaporation' [3], and as we are confident that the scattering originates from phonon–phonon interactions, we have a unique system in which to measure the 4PP.

The dispersion curve of phonons in He II has been measured directly by neutron scattering. The neutron scattering linewidths are related to the lifetimes of the excitations, which are due to both decays and scattering with other ambient excitations [4]. For low- and high-frequency phonons these linewidths are too small to measure when $T < 1.2$ K. The lifetimes of medium frequency (5.5 K $< \hbar\omega/k_B <$ 8.5 K) phonons can be measured using neutron spin-echo techniques [5]. The shortness of the lifetimes of these phonons is due to the strong three-phonon ($p_1 \rightarrow p_2 + p_3$) decays allowed by the anomalous dispersion (upward curvature of $\omega(q)$) in this frequency region. At low temperatures, the 4PP rate is far too small to be obtained from measurements of the neutron scattering linewidths.

Four-phonon scattering ($p_1 + p_2 \rightarrow p_3 + p_4$) in liquid helium was studied theoretically to describe the viscosity of the fluid [6], and the attenuation of sound via relaxation processes in the phonon 'gas' [7]. When these calculations were published, the dispersion of phonons in He II was believed to curve downwards at all frequencies, so three-phonon interactions were forbidden and the four-phonon interactions dominated. However, we now know that there is anomalous dispersion which gives a strong interaction by the three-phonon process (3PP). Because the 3PP rate varies approximately as q^5 [8] up to a frequency limit at $\hbar\omega_c^{(3)}/k_B = 8.6$ K (estimated from neutron scattering data [9]), it is weak for low-frequency phonons, and for these phonons, the four-phonon process (4PP) must also be considered. At the high-frequency end of the phonon spectrum, the 3PP is strictly forbidden for phonons with $\omega > \omega_c^{(3)}$. Spontaneous decay into a multitude of low-frequency phonons is possible for phonons with frequencies up to $\omega_c^{(\infty)}$, where $\hbar\omega_c^{(\infty)}/k_B = 10$ K. So we have high-frequency ($\hbar\omega/k_B > 10$ K) phonons which are stable against spontaneous decay, and their only significant interaction, for $T < 0.5$ K, is four-phonon scattering.

It is now possible to study the attenuation of these high-frequency phonons using quantum evaporation, where only excitations with energy greater than the binding energy of a helium atom to the liquid (7.16 K) can create a detectable signal at a receiver in the vapour. The purpose of this paper is to describe the attenuation of these signals in terms of four-phonon scattering where the high-frequency injected phonon collides with a low-frequency thermal phonon and creates two final-state phonons. First, the method used in [6, 10] to obtain the four-phonon scattering rate is outlined to highlight the assumptions and simplifications made.

2. Review of Landau and Khalatnikov's theory

The liquid Hamiltonian as a function of density is given by

$$E(\rho) = \int H(\rho)\,\mathrm{d}V \tag{1}$$

where $H(\rho)$ is the local energy density

$$H(\rho) = \frac{(\rho_0 + \rho')v \cdot v}{2} + \frac{c^2\rho'^2}{2\rho_0} + \frac{1}{3!}\frac{\partial}{\partial\rho}\left(\frac{c^2}{\rho}\right)\rho'^3 + \frac{1}{4!}\frac{\partial^2}{\partial\rho^2}\left(\frac{c^2}{\rho}\right)\rho'^4 + \ldots \tag{2}$$

where c is the ultrasonic velocity, v is the fluid velocity, ρ_0 is the equilibrium liquid density, ρ is the time- and space-dependent density, and $\rho' = \rho - \rho_0$ is the density perturbation from equilibrium [6]. For a quantum description, v and ρ' can be expressed in terms of the phonon creation (a^+) and annihilation (a) operators,

$$v(r) = \frac{1}{\sqrt{V}} \sum_q \left(\frac{\hbar\omega}{2\rho_0}\right)^{1/2} e_q \left(a_q \exp\{i(q\cdot r - \omega t)\} + a_q^+ \exp\{-i(q\cdot r - \omega t)\}\right) \quad (3)$$

$$\rho'(r) = \frac{1}{\sqrt{V}} \sum_q \left(\frac{\hbar\rho_0}{2\omega}\right)^{1/2} q \left(a_q \exp\{i(q\cdot r - \omega t)\} + a_q^+ \exp\{-i(q\cdot r - \omega t)\}\right) \quad (4)$$

where $[a_j, a_k^+] = \delta_{jk}$ and e_q is the unit vector in the direction of the momentum. Terms in the Hamiltonian which are to nth order in the quantum operators correspond to interaction vertices involving n phonons.

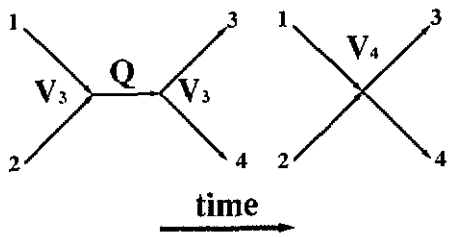

Figure 1. Two possible routes by which two incoming phonons can interact and produce two different outgoing phonons.

Until now, only two routes of the four-phonon interaction have been actively considered in He II, and these are shown in figure 1. The second of these two diagrams (the four-phonon point vertex) was neglected in favour of the much stronger process represented by the first diagram. In second-order perturbation theory, the matrix element for the single remaining diagram is given by

$$M = \frac{1}{\hbar} \sum_Q \frac{\langle q_4 q_3 | V_3 | Q \rangle \langle Q | V_3 | q_1 q_2 \rangle}{\omega(q_1) + \omega(q_2) - \omega(Q)} \quad (5)$$

where

$$V_3 = \rho' v \cdot v/2 + (1/3!)(\partial/\partial\rho)(c^2/\rho)\rho'^3. \quad (6)$$

The wavevector of the intermediate state is determined by the conservation of momentum such that

$$Q = q_1 + q_2 = q_3 + q_4. \quad (7)$$

Because the matrix element becomes large for incoming phonons with parallel momenta due to the denominator in equation (5), Landau and Khalatnikov [6] calculate the cross section (using Fermi's Golden Rule) by integrating only over small angles between the two incoming phonons, and assume that this is the dominant contribution. The cross section for a high-frequency phonon in a region of low-frequency thermal phonons is given as [6, 10]

$$\sigma(q_1) = (u+1)^4 q_1^4 / [\pi(24\rho_0 c)^2 \gamma] \quad (8)$$

where q_1 is the wavevector of the high-frequency phonon, $\gamma = 3 \times 10^{47}$ s^2 kg^{-2} m^{-2} is the dispersion parameter in

$$\omega = c_0 q(1 - \gamma \hbar^2 q^2) \tag{9}$$

and

$$u = (\rho/c)(\partial c/\partial \rho) = 2.84 \tag{10}$$

is the Grüneisen parameter given by experiment [11]. The mean free paths l obtained from $l = (n\sigma)^{-1}$, where n is the number density of thermal phonons, are shown in figure 2. For $T = 100$ mK, these path lengths are less than 0.1 mm.

If the two incoming phonons in a four-phonon interaction have parallel momenta, then the momentum of the high-frequency outgoing phonon must be greater than the momentum of the high-frequency ingoing phonon. For anti-parallel collisions, the high-frequency outgoing phonon has a smaller momentum than the ingoing high-frequency phonon. In parallel collisions, the density of final states is small, but the matrix element is large because of the small denominator in equation (5). In anti-parallel collisions, the matrix element is smaller but the density of final states is larger. Therefore, it can be argued that these two effects compensate for each other to give a final-state phonon that has nearly the same frequency and direction as the high-frequency ingoing phonon. This is because a small but finite angle between the two incoming phonons allows some down-scattering which is enhanced by the density of final states. Consequently many interactions would be necessary for a high-frequency phonon to be lost from a collimated beam, either by small angular changes or by energy loss to below the threshold of stability against decay [12].

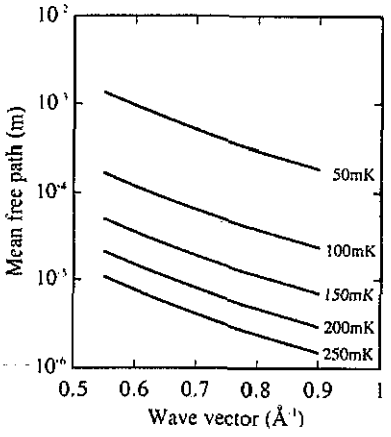

Figure 2. The mean free path for high-frequency phonons as a function of wavevector in a distribution of ambient thermal phonons at the temperature shown, according to [6].

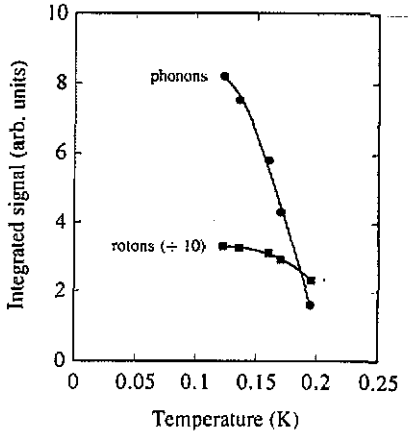

Figure 3. The dependence upon ambient liquid temperature of evaporation signals for high-frequency phonons and rotons from 2.5 mW mm^{-2}, 10 μs heat pulses. The roton signal has been scaled down by a factor of 10. The liquid path length is 4.3 mm and the total path length is 7.7 mm. Reproduced from [13].

The first experiments on the evaporation of atoms by high-frequency phonons have shown that for a liquid path length of 4.3 mm, the signal is significantly attenuated in the temperature range between 120 mK and 200 mK, as shown in figure 3 [13]. This temperature dependence can be modelled using the mean free paths shown in figure 2 by assuming an average angular change and energy change of the high-frequency phonon at each interaction [12]. However, while attempting to calculate accurate values for these angular and energy changes, an important shortcoming of the theory came to light. Diagrams that were previously assumed to be negligible were in fact comparable in magnitude with the major term considered by Landau and Khalatnikov. We were influenced in this work by the theory of roton–phonon scattering [14].

In the next section, the matrix element is expanded to include all the possible single intermediate states. The simulated attenuation of phonon evaporation signals is then compared with new experimental results which are extended to lower temperatures than previously obtained, for a range of liquid path lengths.

3. Theory

The four-phonon scattering rate is now obtained by including all of the diagrams that were initially considered in [6]. Diagrams containing two or more intermediate states are expected to be unimportant in this calculation because the series expansion in equation (2) is assumed to converge. If the four phonons in the interaction are specified, then the matrix element for four-phonon scattering will consist of the terms due to the diagrams shown in figure 4, and can be written as

$$M_{2\to 2} = \sum_{\text{all routes}} M \simeq M_A + M_B + M_C + M_4 \tag{11}$$

where $M_{2\to 2} = \langle q_3 q_4 | H | q_1 q_2 \rangle$ represents the matrix element for two initial phonons scattering to form two final phonons.

The first two diagrams include the term considered in earlier versions of the four-phonon scattering theory

$$M_A = \frac{1}{\hbar}\left\{ \frac{\langle q_3 q_4 | V_3 | Q \rangle \langle Q | V_3 | q_1 q_2 \rangle}{\omega(q_1) + \omega(q_2) - \omega(Q)} + \frac{\langle \Omega | V_3 | q_1 q_2 Q \rangle \langle Q q_3 q_4 | V_3 | \Omega \rangle}{-\omega(q_1) - \omega(q_2) - \omega(Q)} \right\} \tag{12}$$

where V_3 is given by equation (6), Q is given by equation (7) for the first contribution in the curly brackets and $|\Omega\rangle$ is the 'vacuum' state representing the system without phonons. The second contribution arises from the reversal of the time ordering of the interaction vertices and so the direction of the intermediate state Q is reversed.

The second pair of diagrams involves a propagator which transfers energy and momentum from one phonon to the other.

$$M_B = \frac{1}{\hbar}\left\{ \frac{\langle q_4 | V_3 | q_2 Q \rangle \langle Q q_3 | V_3 | q_1 \rangle}{\omega(q_1) - \omega(q_3) - \omega(Q)} + \frac{\langle q_3 | V_3 | q_1 Q \rangle \langle Q q_4 | V_3 | q_2 \rangle}{\omega(q_2) - \omega(q_4) - \omega(Q)} \right\} \tag{13}$$

where $Q = q_1 - q_3 = q_4 - q_2$ for the first contribution in the curly brackets and $Q = q_3 - q_1 = q_2 - q_4$ for the second contribution.

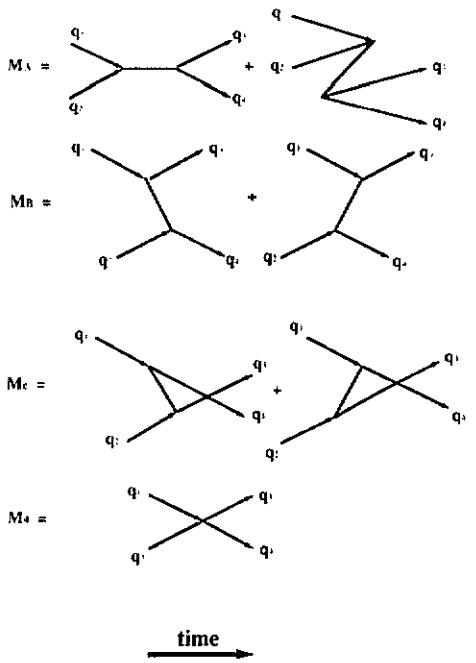

Figure 4. The routes of the four-phonon scattering process considered in this paper. The intermediate states can go either forward or backward in time as described in the appendix.

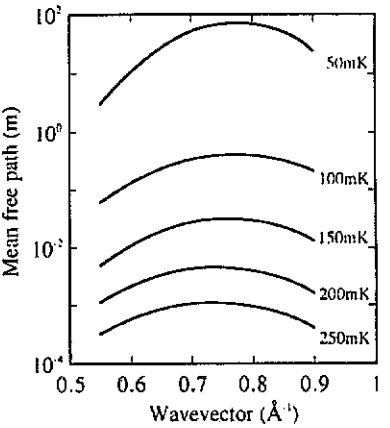

Figure 5. The mean free path between transitions for a high-frequency phonon, calculated from the diagrams shown in figure 4 as a function of phonon wavevector at the indicated ambient liquid temperatures.

The third pair of diagrams is very similar to the second, but with the labels 3 and 4 exchanged, and results from the sum over intermediate states in the expression for the matrix element.

$$M_C = \frac{1}{\hbar}\left\{\frac{\langle q_3|V_3|q_2Q\rangle\langle Qq_4|V_3|q_1\rangle}{\omega(q_1)-\omega(q_4)-\omega(Q)} + \frac{\langle q_4|V_3|q_1Q\rangle\langle Qq_3|V_3|q_2\rangle}{\omega(q_2)-\omega(q_3)-\omega(Q)}\right\} \quad (14)$$

where $\pm Q = q_1 - q_4 = q_3 - q_2$.

Finally, the fourth diagram is the four-phonon point vertex which is given by

$$M_4 = \langle q_3 q_4|V_4|q_1 q_2\rangle \quad (15)$$

where

$$V_4 = (1/4!)(\partial^2/\partial\rho^2)(c^2/\rho)\rho'^4. \quad (16)$$

The expressions for V_n are readily evaluated in terms of the Grüneisen constant using the relations

$$(\partial/\partial\rho)(c^2/\rho) = (c^2/\rho^2)(2u-1) \quad (17)$$

$$(\partial^2/\partial\rho^2)(c^2/\rho) = 2(c^2/\rho^3)(u-1)^2. \quad (18)$$

The complete expressions for each of the terms in the matrix element are given in the appendix.

The transition rate for the injected high-frequency phonon q_1 is calculated using Fermi's Golden Rule

$$\Gamma_1 = \frac{2\pi}{\hbar} \sum_{q_2,q_3} |M_{2\to 2}|^2 \rho(E) \tag{19}$$

where q_4 is fixed by momentum conservation, $\rho(E)$ is the density of final states in an energy interval $\mathrm{d}E$, and where $E = \hbar\omega_{\mathrm{TOT}} = \hbar(\omega_1 + \omega_2)$ is the total energy of the interaction. Double counting is avoided because q_3 is defined to be the high-frequency outgoing phonon such that $q_3 > q_4$ always. The mean free path λ for a chosen high-frequency phonon q_1, with group velocity v_1 is then given simply by

$$\lambda = v_1/\Gamma_1. \tag{20}$$

At this juncture, it is instructive to estimate the importance of these extra terms in the matrix element. In doing so, it is necessary to choose one particular situation where all four phonons are specified. As stated earlier, the most probable outcome was previously assumed to be where little energy and momentum was exchanged between the phonons [12], and this is the case that is now investigated. Phonon q_1 is taken as the incoming high-frequency phonon, q_2 as the thermal phonon, q_3 is the outgoing high-frequency phonon, and q_4 the outgoing low-frequency phonon. So q_1 and q_3 are approximately parallel, whereas q_2 and q_4 are at arbitrary angles. With some simplifications, the matrix element can be written as

$$M_{2\to 2} \propto 2u^2 \left\{ \frac{\omega_{\mathrm{A}}^2}{(\omega_1+\omega_2)^2 - \omega_{\mathrm{A}}^2} + \frac{\omega_{\mathrm{B}}^2}{(\omega_1-\omega_3)^2 - \omega_{\mathrm{B}}^2} + \frac{\omega_{\mathrm{C}}^2}{(\omega_1-\omega_4)^2 - \omega_{\mathrm{C}}^2} \right\} + (u-1)^2 \tag{21}$$

where the subscripts A, B, and C refer to the intermediate state in that diagram. The wavevectors of the intermediate states can be approximated such that

$$(\omega_1+\omega_2)/\omega_{\mathrm{A}} \cong (q_1+q_2)/[q_1 + q_2(e_1 \cdot e_2)] \tag{22}$$

$$(\omega_1-\omega_3)/\omega_{\mathrm{B}} \cong (e_1 \cdot e_{\mathrm{B}}) \tag{23}$$

$$(\omega_1-\omega_4)/\omega_{\mathrm{C}} \cong (q_1-q_4)/[q_1 - q_4(e_1 \cdot e_4)]. \tag{24}$$

Because q_2, q_4 and q_{B} are low-frequency phonons at arbitrary angles to q_1, then letting each term with a dot product equal zero gives

$$M_{2\to 2} \propto u^2\{q_1/q_2 - 2 - q_1/q_4\} + (u-1)^2 \tag{25}$$

where $q_2 \simeq q_4 \ll q_1$. It can now be seen that in this specific case, the first and third terms are the largest in magnitude, are approximately equal, and give a major cancellation. Also, the fourth term which was previously regarded as unimportant is now almost equal in importance with the first three terms due to this cancellation. Therefore the strength of the four-phonon interaction has been dramatically weakened as suggested by experimental observations.

4. Numerical simulation

The expression for the matrix element given in the previous section contains many terms involving the dispersion relation $\omega(q)$, and the determination of an adequate parametrization of this relationship is the starting point of the analysis. Previously published parametrizations [15, 16] are not sufficiently accurate over the whole phonon spectrum from $q = 0$ to the maxon peak. Neutron scattering measurements provide the data points from which an interpolated analytical expression is found. Using the most precise data for the phonon region [17], a sum of Chebyshev polynomials

$$\omega(q) = \sum_{j=1}^{n} c_j T_j(x) \tag{26}$$

was fitted by a least-squares method, where x varies linearly with q from $x = -1$ at $q = 0$ to $x = +1$ at the maxon peak at $q = 1.13$ Å^{-1}. The coefficients given by this method are $c_1 = +8.4466$, $c_2 = +7.1757$, $c_3 = -1.6274$, $c_4 = -0.2624$, $c_5 = +0.1218$, $c_6 = +0.0085$, and $c_7 = 0.0192$.

The simulation of the phonon evaporation signals was performed in the following way. As each injected high-frequency phonon travels through the liquid, it scatters with other excitations, which for $T < 0.6$ K are predominantly thermal phonons. At each interaction, the energy and direction of motion of the high-frequency phonon will be affected. The mean free path between collisions is given by the transition rates calculated using the expressions for the matrix element as given in the appendix. Due to the complexity of these expressions, the transition rates were evaluated numerically in a computer program, called 'FOURPP'. This program also gives the probability distributions of the wavevector change Δq and angular change θ of the high-frequency phonon in each interaction. A second program, called 'PULSE', samples the distributions of these scattering parameters to follow the progress of each high-frequency phonon in the injected heat pulse through the liquid.

In 'FOURPP', the mean free path of the high-frequency phonon is calculated for each value of the liquid temperature (50 mK $< T <$ 250 mK), and for each high-frequency phonon wavevector ($q_1 \geqslant 0.55$ Å^{-1}). A thermal phonon is then randomly selected from an isotropic thermal distribution. These two phonons specify the total energy $\hbar\omega_{TOT}$ and wavevector q_{TOT} of the interaction. The wavevector range of allowed interaction products describes a surface of revolution about q_{TOT}. The shape of this surface is determined solely by the dispersion curve (if the dispersion was linear, then this surface would be an ellipsoid with its foci separated by q_{TOT}).

For each element of this surface, there exists a partial transition rate for the production of the outgoing phonons which form this surface element. Summing over all the elements of the surface gives the total transition rate for an interaction between the two specified incoming phonons. To avoid double counting of final states, this sum is taken over one half of the total surface such that q_3 is always greater than q_4. Averaging over the distribution of thermal phonons gives the transition rate for a high-frequency phonon of wavevector q_1 travelling through a thermal distribution at temperature T. The results of this procedure are shown in figure 5. It can be seen that when all the contributions (to first order in intermediate states) to the matrix element for four-phonon scattering are included, the mean free paths are calculated to be three to four orders of magnitude greater than those of the earlier theory shown

in figure 2. This is due to cancellations between the terms in the expression for the matrix element. The numerical simulation described above was repeated using only the two diagrams shown in figure 1, and this gave a dependence on q of the mean free path similar to that shown in figure 5, but of the same order of magnitude as the curves shown in figure 2. Therefore it is assumed that the dependence on q shown in figure 2 arises from the simplifications made in the calculation of the cross section in the earlier work [6]. The Landau–Khalatnikov theory only considered forward scattering whereas in the present work all directions are considered. There is a large density of states for backscattering which increases the scattering rate as q_1 decreases.

At each liquid temperature T, and for each initial wavevector q_1, a 30×30 array $P(\Delta q, \theta)$ was created by 'FOURPP', where $\Delta q = q_3 - q_1$ and $\cos\theta = e_1 \cdot e_3$. Each pair of final states has a corresponding transition rate associated with a wavevector change Δq and angular shift θ of the high-frequency phonon. The array element into which this point falls is incremented by this rate. After summing over final states and averaging over thermal phonons, each array is normalized such that the sum of all the entries is unity. Each array element then contains the relative probability that the final state occurs with that value of Δq and θ.

These arrays are sampled by 'PULSE', which simulates the propagation of phonons through the liquid. The attenuation is evaluated at the same temperatures as those used in calculating the mean free paths and scattering parameter arrays in 'FOURPP'. Several assumptions have been made.

(i) The high-frequency phonons travel ballistically between collisions with thermal phonons. Interactions with other excitations generated by the heater are ignored because of the short, low-power pulses used in the experiment.

(ii) The high-frequency phonons generated at the heater were assumed to be the tail of a Planck distribution with an effective temperature T_e to be determined.

(iii) Any phonon emerging from a collision with a wavevector less than the stability threshold of $q_c = 0.55$ Å^{-1} (determined from neutron scattering data [17]), decays rapidly to an energy less than the binding energy of helium atoms to the liquid surface. These phonons are deemed to be lost from the evaporation signal before there is a chance of up-scattering in another four-phonon interaction because of strong decay processes [2, 8, 18].

(iv) The probability of quantum evaporation is the same for all phonons with energy greater than the binding energy.

The results of this simulation are presented in figure 7, together with the experimental measurements.

5. Experiment

Liquid ^{4}He was condensed into a brass cell cooled to a base temperature of about 50 mK by a dilution refrigerator. ^{4}He, which contained less than one part in 10^{12} ^{3}He atoms, was condensed into the cell. The temperature of the cell was varied by applying an electrical current to a heater in the mixing chamber of the dilution unit and allowing the cell temperature to reach equilibrium. The temperature was measured using a pre-calibrated Lakeshore germanium resistance thermometer submerged in the liquid in the experimental cell.

Non-thermal excitations were injected into the liquid by the Joule heating of a 1 mm^2 gold film heater submerged in the liquid. The low heat capacity of the

thin film ensured a short time constant of the order of tens of nanoseconds [19]. Previous experiments have shown that approximately 99% of the energy injected into the liquid is in the form of low-frequency phonons, about 0.5% in the form of high-frequency phonons, and about 0.5% as rotons [19]. At the liquid surface, the injected high-energy excitations can each eject a single helium atom into the vapour. For pulse lengths greater than 0.3 μs, the high-frequency phonon evaporation signals are strongly attenuated by scattering processes in front of the heater, and detected signals are dominated by the R^+ (positive group velocity) rotons produced [20]. To study phonon evaporation signals, a 10 mW heater pulse of 0.2 μs duration was used.

Above the liquid ^{4}He surface is a 1 mm^2 zinc film bolometer which is vertically above and facing the heater. The bolometer detects the energy deposited on its surface by atoms evaporated from the bulk liquid surface. The bolometer is maintained at a point on its superconducting transition curve by Joule heating from a negative feedback bridge amplifier [21]. The transition temperature of the zinc is suppressed from $\simeq 0.85$ K to $\simeq 0.3$ K to avoid excessive heat input to the experimental cell by applying an external magnetic field parallel to the film. For the small energy fluxes at the bolometer in this experiment, the decrease in voltage feedback is proportional to the energy flux. These variations in voltage feedback are amplified and electronically captured as a digitized waveform in 1024 channels by a Biomation 8100 which is triggered by the pulse to the heater. Because the signal is typically less than the electronic noise, the waveform is averaged for up to 10^5 repetitions.

Between the heater and bolometer are four horizontal sheets of mica, each 0.12 mm thick and with circular collimating holes of 0.6 mm diameter. The collimation is present to block the paths of excitations which are originally emitted by the heater at large angles to the vertical. With no collimation present, the signals are appreciably broader in time due to the greater number of long-distance, multiply scattered, paths which are allowed.

A selection of detected evaporation signals from 10 mW, 0.2 μs heater pulses for a liquid path length of 10.2 ± 0.1 mm are shown in figure 6 at different ambient liquid temperatures. The reduction in signal with increasing temperature is attributed to the scattering of the high-frequency injected phonons with the thermal phonons in the bulk liquid because the detection efficiency of the bolometer is relatively independent of the ambient temperature [16]. The arrival time of the signal peak indicates that it is due to $\hbar\omega/k_B \simeq 10$ K phonons. Because these phonons are close to the threshold of stability against multiphonon decay [2, 18], the peak of the signal is attenuated more rapidly than the tail which is due to slower phonons of higher frequency.

The phonon evaporation signal is integrated over the region of the peak to minimize the effects of baseline drift. The roton contribution to the evaporation signal is only significant when the vacuum path length is small, due to the refraction of the signal path away from the normal to the liquid surface (in quantum evaporation, energy and momentum parallel to the liquid surface are conserved). This small roton contribution is observed at temperatures $\simeq 0.2$ K for the liquid path length of 15.6 mm, and is approximately independent of temperature up to $T \simeq 0.25$ K. So, a constant value for the integrated roton contribution is subtracted from the integrated phonon signal at all temperatures only for the liquid path length of 15.6 mm. Possible errors introduced by this subtraction procedure will not significantly affect the temperature dependence of the phonon evaporation signal. The results are shown in figure 7 as a function of temperature at three liquid path lengths. The vertical separation of the heater and bolometer is the same value of 15.7 mm in all three cases. For increasing

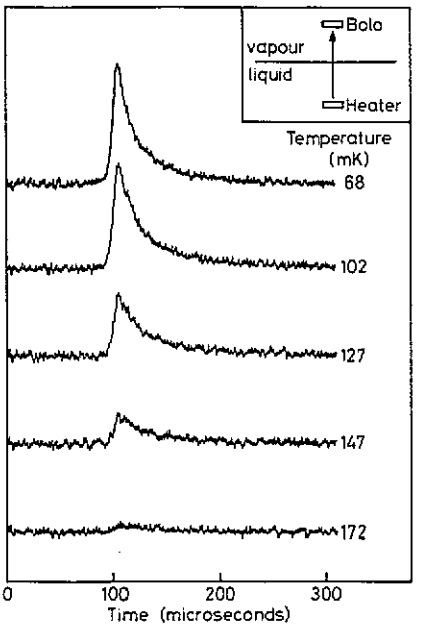

Figure 6. Selected evaporation signals at the indicated liquid temperatures for the arrangement shown schematically inset, from 10 mW mm^{-2} heater pulses of 0.2 μs duration. The liquid path length is 10.2 mm; the total path length is 15.7 mm.

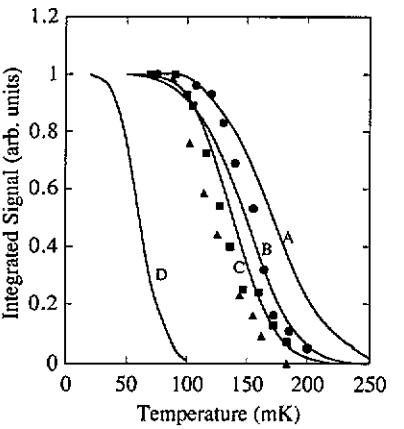

Figure 7. The integrated phonon evaporation signal as a function of liquid temperature for a total path length of 15.7 mm. The experimental data are for liquid path lengths (●) 5.0 mm, (■) 10.2 mm, and (▲) 15.6 mm. The simulation results are for liquid path lengths (A) 5.0 mm, (B) 10.2 mm, and (C) 15.6 mm. Curve D is the result obtained using only the diagrams shown in figure 1 for a liquid path length of 10.2 mm. The data and curves are scaled to be equal to the lowest temperature.

liquid path lengths, the signal is attenuated more rapidly with temperature due to the greater probability of phonon scattering in the liquid. The number density of atoms in the vapour is so low that a negligible number of atom–atom collisions occur in the space above the liquid.

Also shown in figure 7 are the results from the pulse simulation program 'PULSE' described in the previous section, for the same liquid path lengths used in the experiment. The effective temperature T_e of the phonon distribution is taken to be 0.7 K. The agreement is considerably better than with the older incomplete version of the theory. For comparison, curve D is the simulated attenuation for a liquid path length of 10.2 mm, calculated in exactly the same fashion as above, but using only the two diagrams shown in figure 1. The only two parameters in the model that can, to some extent, be varied are T_e and q_c; all the other parameters in the model are relatively well defined. The long-wavelength limit of the Grüneisen parameter has been used in these calculations because an accurate wavevector dependence of the Grüneisen parameter is not available [22].

The effective temperature of the phonon spectrum emitted by a heater at high pressures (where phonon decays are prohibited) has been measured to be $\simeq 0.7$ K at heater powers similar to that used here [23]. This temperature only describes the

shape of the phonon spectrum and not the phonon number density which is determined by the heater power. So, we assume in this work that at the saturated vapour pressure where phonon decays are allowed, the spectrum of the stable high-frequency phonons is described by this value of effective temperature. We find that increasing the effective temperature of the phonon spectrum worsens the agreement between the measurements and the simulation, so we have not included any contribution to the injected phonons from the elastic channel between the heater and the liquid helium [19], because that would shift the spectrum to higher phonon frequencies. In fact, better agreement is found for $T_e = 0.5$ K, but as this is lower than previous measurements, we have chosen not to use it for the comparisons presented here.

A value of $q_c \simeq 0.53$ Å^{-1} has been measured directly for phonons propagating over a liquid path length of 1.1 mm [18]. Using this value of q_c gives a marginally better fit to the data; however, it is unclear whether this decay cut-off has the same value for these longer liquid path lengths.

Although the agreement between the simulated and experimental attenuation curves is not perfect, the theoretical interaction rate is now weaker than the experimental rate. The theoretical rate could now be increased by extending the matrix element to include higher-order diagrams in the four-phonon scattering process (involving multiple propagators). The inclusion of higher-order scattering processes where two phonons collide to produce three or more final-state phonons should also increase the scattering rate and improve the agreement even further.

6. Summary

The hydrodynamic theory of four-phonon scattering has been extended to include further terms in the matrix element. These extra terms, which have previously been disregarded as unimportant, give significant cancellations with the leading term which was the only term previously considered. The density of final states favours a large transfer of momentum and energy from the high-frequency incoming phonon to the low-frequency incoming phonon. This is not significantly modified by the matrix element, which is at variance with earlier calculations based only on the single leading diagram. It is found that the mean free path for high-frequency phonons in He II is approximately three orders of magnitude larger than previous theoretical estimates. With no free parameters in the calculations, this analysis of four-phonon scattering gives good agreement with the experimental measurements in the temperature range considered. It is believed that this is the first quantitative agreement of the theory of four-phonon scattering in any material with experimental measurements.

Acknowledgments

This work was completed with the support of the SERC. Helpful and interesting conversations were held with Professor J C Inkson and Dr G P Srivastava. Technical assistance was provided by Mr M Gear.

Appendix

The complete expressions for the terms in the matrix element are

$$M_A = (\hbar^2/8\rho_0 V)[n_1 n_2(n_3+1)(n_4+1)]^{1/2}\exp\{-i(\omega_1+\omega_2-\omega_3-\omega_4)t\}$$
$$\times\left\{\frac{\delta(q_1+q_2-Q)\delta(Q-q_3-q_4)}{(\omega_1+\omega_2-\omega_Q)}+\frac{\delta(q_1+q_2+Q)\delta(Q+q_3+q_4)}{(-\omega_1-\omega_2-\omega_Q)}\right\}$$
$$\times\left\{\left(\frac{\omega_1\omega_2}{\omega_Q}\right)^{1/2}Q(e_1\cdot e_2)+\left(\frac{\omega_1\omega_Q}{\omega_2}\right)^{1/2}q_2(e_1\cdot e_Q)\right.$$
$$\left.+\left(\frac{\omega_2\omega_Q}{\omega_1}\right)^{1/2}q_1(e_2\cdot e_Q)+c^2(2u-1)\frac{Qq_1q_2}{(\omega_Q\omega_1\omega_2)^{1/2}}\right\}$$
$$\times\left\{\left(\frac{\omega_3\omega_4}{\omega_Q}\right)^{1/2}Q(e_3\cdot e_4)+\left(\frac{\omega_3\omega_Q}{\omega_4}\right)^{1/2}q_4(e_3\cdot e_Q)\right.$$
$$\left.+\left(\frac{\omega_4\omega_Q}{\omega_3}\right)^{1/2}q_3(e_4\cdot e_Q)+c^2(2u-1)\frac{Qq_3q_4}{(\omega_Q\omega_3\omega_4)^{1/2}}\right\} \tag{A1}$$

$$M_B = (\hbar^2/8\rho_0 V)[n_1 n_2(n_3+1)(n_4+1)]^{1/2}\exp\{-i(\omega_1+\omega_2-\omega_3-\omega_4)t\}$$
$$\times\left\{\frac{\delta(q_1-q_3-Q)\delta(Q+q_2-q_4)}{(\omega_1-\omega_3-\omega_Q)}+\frac{\delta(q_1-q_3+Q)\delta(Q-q_2+q_4)}{(\omega_2-\omega_4-\omega_Q)}\right\}$$
$$\times\left\{\left(\frac{\omega_1\omega_3}{\omega_q}\right)^{1/2}Q(e_1\cdot e_3)+\left(\frac{\omega_1\omega_Q}{\omega_3}\right)^{1/2}q_3(e_1\cdot e_Q)\right.$$
$$\left.+\left(\frac{\omega_3\omega_Q}{\omega_1}\right)^{1/2}q_1(e_3\cdot e_Q)+c^2(2u-1)\frac{Qq_1q_3}{(\omega_Q\omega_1\omega_3)^{1/2}}\right\}$$
$$\times\left\{\left(\frac{\omega_2\omega_4}{\omega_Q}\right)^{1/2}Q(e_2\cdot e_4)+\left(\frac{\omega_2\omega_Q}{\omega_4}\right)^{1/2}q_4(e_2\cdot e_Q)\right.$$
$$\left.+\left(\frac{\omega_4\omega_Q}{\omega_2}\right)^{1/2}q_2(e_4\cdot e_Q)+c^2(2u-1)\frac{Qq_2q_4}{(\omega_Q\omega_2\omega_4)^{1/2}}\right\} \tag{A2}$$

$$M_4 = \frac{\hbar^2c^2(u-1)^2}{2\rho_0 V}\frac{q_1q_2q_3q_4}{(\omega_1\omega_2\omega_3\omega_4)^{1/2}}[n_1n_2(n_3+1)(n_4+1)]^{1/2}\delta(q_1+q_2-q_3-q_4)$$
$$\times\exp\{-i(\omega_1+\omega_2-\omega_3-\omega_4)t\}. \tag{A3}$$

The expression for M_C (the 'exchange' diagram [24]) is not printed here because it is similar to M_B apart from the interchange of subscripts 3 and 4.

The expressions for M_A, M_B and M_C would contain a factor of n_Q+1 if only the intermediate states created at the first vertex and annihilated at the later vertex

(the arrow of the intermediate state going forward in time) are considered. If the intermediate state is first 'borrowed' from the ambient distribution and then replaced by creation at the later vertex (arrow going backwards in time), these contributions contain a factor of n_Q. Because the denominators have opposite sign in these two cases, the n_Q-factor is removed by the summation over intermediate states [1].

References

[1] Ecsedy D J and Klemens P G 1977 *Phys. Rev.* B **15** 5957
[2] Dynes R C and Narayanamurti V 1974 *Phys. Rev. Lett.* **33** 1195
[3] Baird M J, Hope F R and Wyatt A F G 1983 *Nature* **304** 325
[4] Mezei F 1980 *Phys. Rev. Lett.* **44** 1601
[5] Mezei F, Lartigue C and Farago B 1991 *Excitations in 2D and 3D Quantum Fluids* (New York: Plenum)
[6] Landau L D and Khalatnikov I M 1949 *Sov. Phys.-JETP* **19** 637
[7] Khalatnikov I M and Chernikova D 1966 *Sov. Phys.-JETP* **22** 1336
[8] Slukin T J and Bowley R H 1974 *J. Phys. C: Solid State Phys.* **7** 1779
Maris H J 1974 *Phys. Rev.* A **9** 1412
[9] Stirling W 1983 *Proc. 75th Jubilee Conf. on ^{4}He* ed J G M Armitage (Singapore: World Scientific) p 109
[10] Khalatnikov I M 1965 *An Introduction to the Theory of Superfluidity* (New York: Benjamin)
[11] Abraham B M, Eckstein Y, Ketterson J B, Kuchnir M and Roach P R 1970 *Phys. Rev.* A **1** 250
[12] Wyatt A F G 1987 *Proc. 18th Int. Conf. on Low Temperature Physics; Japan J. Appl. Phys. Suppl. 3* **26** 7
[13] Baird M, Richards B and Wyatt A 1987 *Proc. 18th Int. Conf. on Low Temperature Physics; Japan J. Appl. Phys. Suppl. 3* **26** 387
[14] Hyman D S, Scully M O and Widom A 1969 *Phys. Rev.* **186** 231
[15] Maris H 1977 *Rev. Mod. Phys.* **49** 341
[16] Brown M 1990 *PhD Thesis* University of Exeter
[17] Stirling W 1985 private communication
[18] Haavasoja T, Narayanamurti V and Chin M 1984 *J. Low-Temp. Phys.* **57** 55
[19] Wyatt A, Lockerbie N and Sherlock R 1989 *J. Phys.: Condens. Matter* **1** 3507
[20] Brown M and Wyatt A 1990 *J. Phys.: Condens. Matter* **2** 5025
[21] Sherlock R and Wyatt A 1983 *J. Phys. E: Sci. Instrum.* **16** 669, 673
[22] Maris H J 1973 *Phys. Rev.* A **8** 1980
[23] Wyatt A F G, Sherlock R A and Allum D R 1982 *J. Phys. C: Solid State Phys.* **15** 1897
[24] Feynman R P 1962 *The Theory of Fundamental Processes* (New York: Benjamin)